CAVITATION PHENOMENA IN THE INJECTION NOZZLE: THEORETICAL AND NUMERICAL ANALYSIS

Martin Volmajer, Breda Kegl
University of Maribor, Faculty of mechanical engineering,
Smetanova ulica 17, SI-2000 Maribor, Slovenia
Phone: +386 2 220 77 38, Phone: +386 2 220 77 32, Fax: +386 2 220 79 90
e-mails: martin.volmajer@uni-mb.si; breda.kegl@uni-mb.si

Abstract

The evaporation of diesel fuel in the injection nozzle significantly influences the injection characteristic and spray formation process. In presented paper the cavitation phenomena in the diesel injection nozzle is analysed. The theoretical backgrounds of the cavitation occurrence presented in the first part of the paper are followed by the numerical analyses of two-phase flow in some simplified nozzle models. The numerical analyses are made using the computational fluid dynamic (CFD) program Fire. The two-phase flow is analysed using the two-equation approach, where all conservation equations are solved for every single phase. Numerical analysis results are compared to the experimental observations of the two-phase flow available from the literature. Results of the numerical analysis are in accordance with those experiments. The results show that higher pressure differences yield more cavitation in the nozzle holes. Results of the geometry variations on the simplified nozzle model showed that the introduction of the chamfer at the hole inlets yield lower cavitation.

Keywords: *two-phase flow, cavitation, injection nozzle, CFD*

1. Introduction

The development of the modern compression ignition engine is mainly connected with rising of injection pressure and the possibility of injecting several jets during the single injection cycle. Both modifications influence positively the engine characteristics and the emission formation processes. At the other side rising of the injection pressure results in higher flow velocities in the nozzle hole channels and in evaporation of fuel in the nozzle holes. The fuel evaporates on the sharp edges at the nozzle hole inlet, where the static pressure falls bellow the fuel vapour pressure. The vapour is spreading along the nozzle hole and can also reach the outlet. The evaporation of fuel and the cavitation[1] process in the nozzle hole significantly influence the in-nozzle flow and the spray formation process (Payri [17], Jung [11], Ganippa [8], Laoonual [14], Baumgarten [4], Soteriou [20]) and it can also cause the erosion of nozzle material when bubbles collapse close to the nozzle wall. Goeschel [10], Nurrick [16] and Melcher [15] where among the first authors who warned against fuel evaporation in the diesel injection nozzle channel and the problems that could results due to cavitation. Some aspects were also presented in [12]. Since the typical diameter of the diesel injection nozzle is usually less than 1 mm and the pressure differences could even exceed 200 MPa, the experimental analyses are quite difficult and limited. The majority of the experimental analysis on the two phase flow in the injection nozzles used to be connected with the measurements and observation on the scaled-up models (Arcoumanis [1], Ganippa [8][9]). In recent years also several observations of two-phase flow on the real size nozzles (Arcoumanis [3], Badock [4], Koenig [13]) or geometries close to real nozzles (Winklhofer

[1] cavitation is usually understood as the formation and collapse of vapour bubbles. Cavus (Latin), hole. [18]

[21]) were performed. Additionally to experimental analysis the computational fluid dynamics programs gained on importance.

Due to the above-mentioned problems the cavitation in the diesel injection nozzles should be analysed more carefully. The cavitation phenomena should be taken into the consideration when designing or improving the injection nozzles and injection systems. The present paper discuses the theory of cavitation occurrence in the diesel injection nozzle and its influence on the nozzle flow characteristics. In the second part also some numerical results of the two-phase flow in the scaled up and real size simplified nozzle models are presented. The results are compared with the experimental results from the literature.

2. Theoretical background

Cavitation bubbles arise because of low static pressure that occurs near a sharp inlet corner in the nozzle flow. If the corner of the inlet is sufficiently sharp, the flow tends to separate and forms a contraction (vena contracta) inside the nozzle, which reduces the area through which the liquid flows. This reduced area is accompanied by an increase in velocity, as predicted by conservation of mass. Conservation of momentum predicts that the acceleration of the liquid through the vena contracta causes a pressure depression in the throat of the nozzle. The low pressure inside the throat of the nozzle may fall below the vapour pressure of the liquid, causing cavitation. A simple sketch of this flow is presented in Figure 2.1. Cavitating flow does not, however, strictly adhere to this simple idealization. The formation of the bubbles is sensitive to the geometry of the corner (sharp, rounded) and to any imperfections in the nozzle shape (i.e. roughness [21]). For example in SAC and the VCO nozzles is the vapour mainly present at the upper part of the nozzle hole and there is always more vapour present in the holes with higher inclination angles (Figure 2.2). The cavitation is also very sensitive for the quality of the liquid (i.e. fuel). That is the number of present nuclei per cubic meter of liquid. Furthermore, cavitation inception may occur at pressures below the vapour pressure. Another complication is that the cavitating flow is transient and fully three-dimensional. The location of the vapour is not steady and it is usually also not symmetrical. [19]

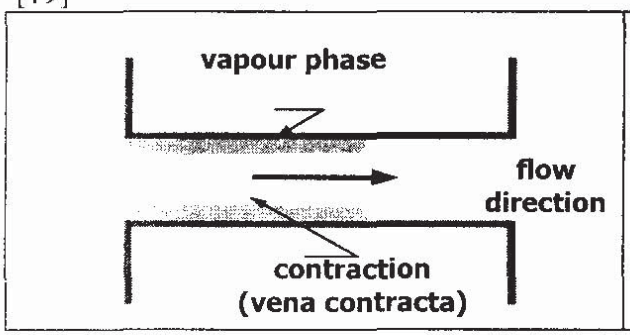

Figure 2.1. Simplified sketch of the cavitation in the nozzle. [19] (Grey represents the vapour phase)

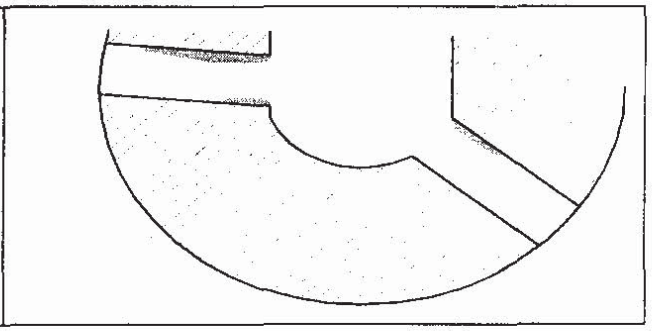

Figure 2.2. Cavitation in SAC nozzle (Grey represents the vapour phase)

From the experiments made by Arcoumanis et.al. [1]-[3] several types of cavitation in the injection nozzle can be observed[2]. In the nozzle hole the fluid starts to evaporate at the sharp inlet edge. Initially a bubbly flow structure was identified followed by the pre-film stage cavitation consisting of a dense bubble cloud and film type cavitation at which complete flow separation takes place at the nozzle hole inlet [1]. Additionally to hole types of cavitation, cavitation strings were observed to form inside the sac volume, which seemed to develop transiently and periodically between adjacent holes [1]. Laoonual et.al. [14] observed three

[2] Actually there is no universal definition of the different types of cavitation flow. The definition is quite subjective and it is also significantly affected by the visualisation procedure.

different types of cavitation in the VCO nozzle: inception cavitation, super cavitation and hydraulic flip. The first one describe the state when the cavitation first appears, the second describes the situation where there is a strong cavitation zone close to the nozzle outlet and the last describes the situation where the liquid jet completely separates from the nozzle wall.

3. Numerical analysis

Numerical analyses were made using the CFD program FIRE. Two-phase flow is calculated with the two-equation model, with a continuous liquid and a dispersed vapour phase [7].

Mass conservation equation:

$$\frac{\partial \alpha_k \rho_k}{\partial t} + \nabla \cdot \alpha_k \rho_k v_k = \sum_{l=1..l\neq k}^{n} \Gamma_{kl} , \tag{2.1}$$

where α_k is volume fraction of phase k, v_k is phase k velocity, and Γ_{kl} represents the interfacial mass exchange between phases k and l. The compatibility condition must be observed:

$$\sum_{k=1}^{n} \alpha_k = 1 . \tag{2.2}$$

Momentum conservation equation:

$$\frac{\partial \alpha_k \rho_k v_k}{\partial t} + \nabla \cdot \alpha_k \rho_k v_k v_k = -\alpha_k \nabla p + \nabla \cdot \alpha_k (\tau_k + T_k') + \alpha_k \rho_k g + \sum_{l=1..l\neq k}^{n} M_{kl} + v_k \sum_{l=1..l\neq k}^{n} \Gamma_{kl} , \tag{2.3}$$

where f is the body force vector which comprises gravity g; M_{kl} represents the momentum interfacial interaction between phases k and l, and p is pressure. Identical pressure is assumed for all phases. The phase k shear stress, τ_k , equals:

$$\tau_k = \mu_k \left[\left(\nabla v_k + \nabla v_k^T \right) - \frac{2}{3} \nabla \cdot v_k \right] , \tag{2.4}$$

where μ_k is molecular viscosity. Reynolds stress T_k' equals:

$$T_k' = -\rho_k \overline{v_k' v_k'} = \mu_k' \left[\left(\nabla v_k + \nabla v_k^T \right) - \frac{2}{3} \nabla \cdot v_k \right] - \frac{2}{3} \nabla \cdot v_k I . \tag{2.5}$$

Turbulent viscosity is modelled as:

$$\mu_k' = \rho_k C_\mu \frac{k_k^2}{\varepsilon_k} . \tag{2.6}$$

Since the analyses in the presented paper were made at the constant temperature the enthalpy conservation equation will not be described in the details here. One can find the description in [7].

Turbulent kinetic energy (TKE) conservation equation:

$$\begin{aligned} &\frac{\partial \alpha_k \rho_k k_k}{\partial t} + \nabla \alpha_k \rho_k v_k k_k = \\ &\nabla \alpha_k \left(\mu_k + \frac{\mu_k'}{\sigma_k} \right) \nabla k_k + \alpha_k P_k + \alpha_k P_{B.k} - \alpha_k \rho_k \varepsilon_k + \sum_{l=1..l\neq k}^{n} K_{kl} + k_k \sum_{l=1..l\neq k}^{n} \Gamma_{kl} \end{aligned} \tag{2.7}$$

Turbulence dissipation equation (TED):

$$\begin{aligned} &\frac{\partial \alpha_k \rho_k \varepsilon_k}{\partial t} + \nabla \cdot \alpha_k \rho_k v_k \varepsilon_k = \nabla \cdot \alpha_k \left(\mu_k + \frac{\mu_k'}{\sigma_\varepsilon} \right) \nabla \varepsilon_k + \sum_{l=1..l\neq k}^{n} D_{TED.kl} + \varepsilon_k \sum_{l=1..l\neq k}^{n} \Gamma_{kl} + \alpha_k C_1 P_k \frac{\varepsilon_k}{k_k} \\ &- \alpha_k C_2 \rho_k \frac{\varepsilon_k^2}{k_k} + \alpha_k C_3 \max(P_{B.k}, 0) \frac{\varepsilon_k}{k_k} - \alpha_k C_4 \rho_k \varepsilon_k \nabla \cdot v_k \end{aligned} \tag{2.8}$$

In two-equation model several mass exchange terms could be introduced (According to the type of two-phase flow.). In the presented analysis the cavitation model is employed.

Mass exchange term is defined with the following equations:

$$\Gamma_c = \frac{1}{C_{CR}} sign(\Delta p) \cdot 3.85 \cdot \frac{\rho_d}{\sqrt{\rho_c}} N'''^{1/3} \alpha_d^{2/3} |\Delta p|^{1/2} \tag{2.9}$$

$$\Gamma_d = sign(\Delta p) \cdot 3.85 \cdot \frac{\rho_d}{\sqrt{\rho_c}} N'''^{1/3} \alpha_d^{2/3} |\Delta p|^{1/2}, \tag{2.10}$$

where the effective pressure difference equals:

$$\Delta p = p_{sat} - (p - C_E \frac{2}{3} \rho_c k_c). \tag{2.11}$$

C_E is the Egler coefficient, which varies between 1 and 1,4. C_{CR} is the condensation reduction factor. N''' is the bubble number density, which is calculated by the assumed diminishing linear ramp:

$$N''' = \begin{cases} N_0''' & \alpha_d \le 0{,}5 \\ 2(N_0''' - 1)(1 - \alpha_d) + 1 & \alpha_d > 0{,}5 \end{cases}, \tag{2.12}$$

where N_0''' represent the initial value of the bubble number density.

Interfacial momentum exchange term is defined with:

$$M_c = C_D \frac{1}{8} \rho_c A_i''' |v_r| v_r + C_{TD} \rho_c k_c \nabla \alpha_d = -M_d \tag{2.13}$$

where v_r is the relative velocity and A_i''' is the interfacial area density for bubbly flow:

$$A_i''' = \pi D_b^2 N''' = (36\pi)^{\frac{1}{3}} \alpha_d^{\frac{2}{3}}. \tag{2.14}$$

C_D is the discharge coefficient:

$$C_D = \begin{cases} \frac{192}{Re_b}(1 + 0.1 Re_b^{0.75}) & Re_b \le 1000 \\ 0.438 & Re_b > 1000 \end{cases} \tag{2.15}$$

C_{TD} is turbulent dispersion coefficient, which value is between 0.05 and 0.5.

3. 1. Scaled up model

Scaled-up model is made according to the dimensions of model used in the experimental analysis presented by Ganippa et.al [8][9]. The dimensions of the scaled-up nozzle model are presented in Figure 3.1 and Table 3.1. Calculations are performed for five different cases, where the pressure difference is varied. The velocity boundary condition is set at the inlet and the pressure boundary condition is set at the outlet. The fluid used in the analysis is water.

Table 3.1. Experimental conditions and boundary conditions for numerical analysis

Case	Δp [MPa]	Re	CN	v_out [m/s]	v_in [m/s]
1	0.1	55860	1	14.1	0.88
2	0.12	61250	1.2	15.5	0.97
3	0.15	68600	1.5	17.3	1.08
4	0.185	75460	1.85	19.2	1.20
5	0.21	78890	2.1	20.5	1.28

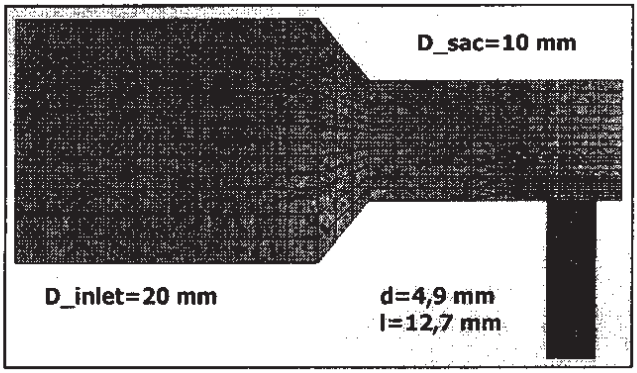

Figure 3.1. Dimensions of the scaled-up nozzle model

3. 2. Simplified real-size nozzle

Dimensions of the simplified real size nozzle model are presented on the following figure. The model is quasi two-dimensional with a depth of 0.1 mm. The symmetry boundary conditions are applied for the left and the right side plane. Analyses were made for 7 different cases. The pressure difference was fixed for all cases. For cases 6-10 the dimensions at the in- and outlet were fixed, while the shape of the hole inlet edges were changed. At cases 11 and 12 the diameters at the in- and outlet were the same as in the previous cases. The inlet edge was sharp, while the length of the hole was 0.45 mm in Case 11 and 1.7 mm in Case 12.

Table 3.2. Boundary conditions and model data for the simplified real-size nozzle model

Δp=19.9 MPa		
Case	r[mm]	l [mm]
6	sharp edge	1
7	0.05	1
8	0.10	1
9	0.15	1
10	0.20	1
11	sharp edge	0.45
12	sharp edge	1.7

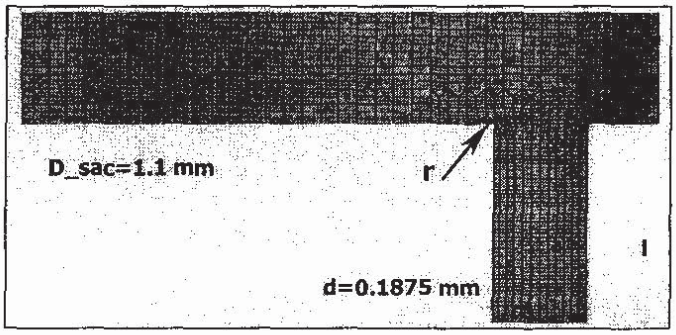

Figure 3.2. Dimensions of the real-size simplified model

4. Results

4. 1. Scaled-up model

The results of the numerical analysis on the scaled-up nozzle model are presented on the following figures. When the numerical results are compared to the experimental observations it has to be considered that the photographs taken from the experimental set-up show the cavitation through the whole nozzle. In contrast to this, the results of the numerical analysis always cover a certain layer. To obtain comparable figures, the results at different cuts have to be superimposed. This is shown in Fig. 4,1 where surface values as well as several cuts for the vapour volume fraction are depicted together with the reconstruction of the superimposed view. However, in the comparisons shown below always single cuts have been used. Thus, the total vapour volume fraction from the calculation is expected to be somewhat larger. Since the results of numerical analyses are presented on the red-blue scale it should be mentioned for black and white prints that the nearly black colours represent the liquid phase, while the vapour is represented with grey shades. Dark grey represent the values of vapour fraction about 1 and the light grey shows the values between 0 and 1.

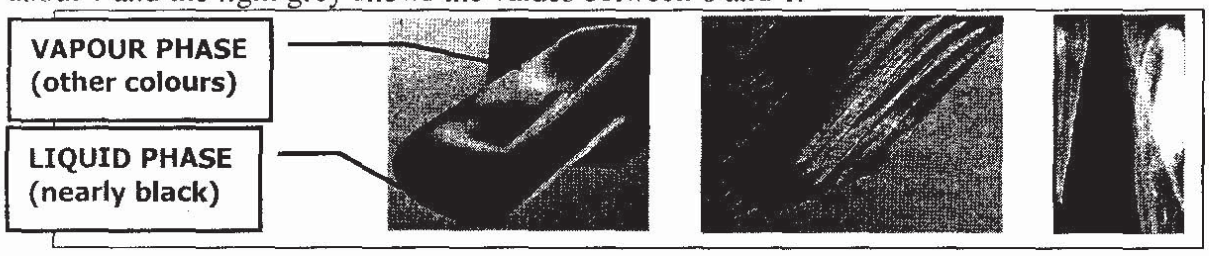

Figure 4.1. Vapour distribution in the nozzle hole – case 5 (left: surface view, centre: cuts view (grey: vapour, black: liquid), right: view through several cuts)

Figure 4.2 shows the photographs of the experimental observations [8], while figures 4.3 and 4.4 show the results of the numerical analysis. The comparison of both analyses shows that the numerical analysis does not completely represent the experimental results. But, it can be also stated that the model predicts the evaporation of water at the same places as

observed at the experimental observations. In Case 1 the majority of vapour phase is present at the upper part of the nozzle hole, while the area at the lower part is significantly smaller. This is in accordance with the experimental observation, where the vapour is present mainly at the upper part. The results of other cases show that the higher pressure difference yields a larger amount of vapour present in the nozzle hole. In Case 5 the vapour even reaches the nozzle outlet. This phenomenon significantly influences the spray formation what was well observed by the Ganippa et.al. [8][9], von Berg et.al. [6] and Koenig et.al.[13].

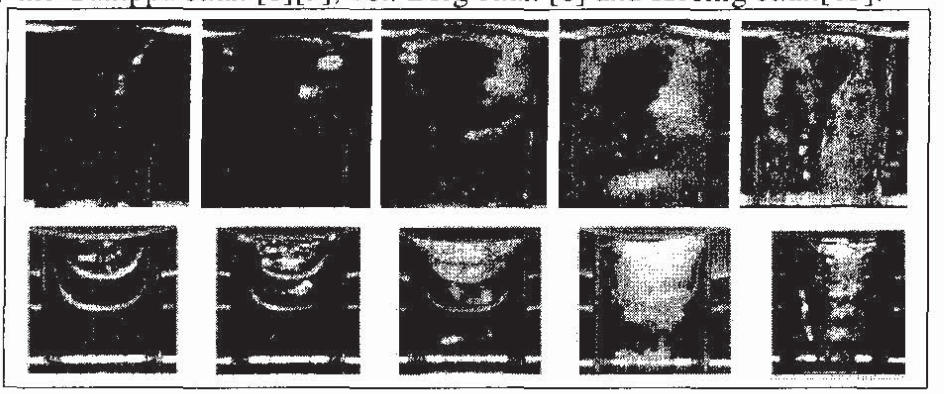

Figure 4.2. Photo of the two-phase nozzle flow – First row: side view, second row: top view (from left: case 1-5, Scaling: white-grey: vapour, Black: liquid), Ganippa [8]

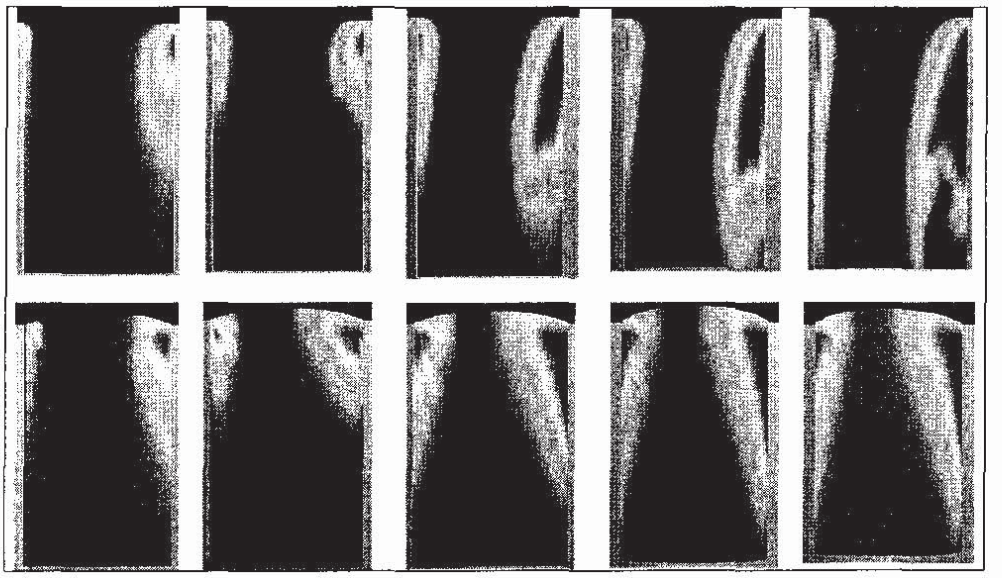

Figure 4.3. Vapour volume fraction in the nozzle hole channel (first row: side view – cut y=0, second row: surface view, from left: case 1-5)

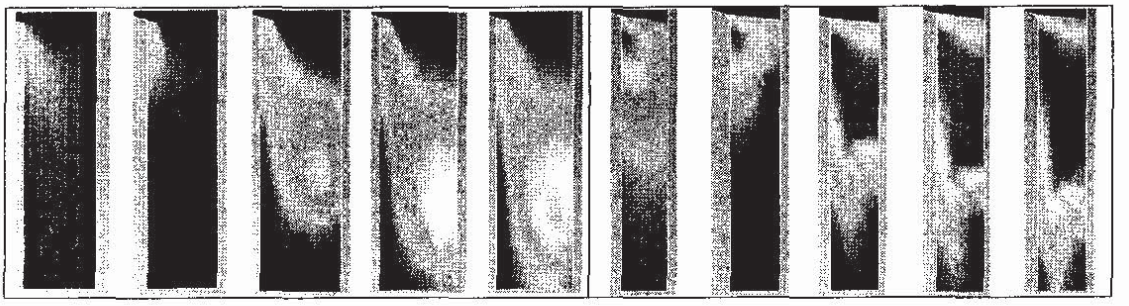

Figure 4.4. Vapour volume fraction in the nozzle, top view – cut z=0,038 (from left: case 1-5)

Figure 4.5. Vapour vol. fraction in the nozzle, top view–cut z=0,039 (from left: case 1-5)

4. 2. Simplified real-size nozzle

Vapour volume fraction distribution in the simplified real size nozzle is presented on Fig. 4.6. Considering the observation of the results with respect to colours, the same explanations as at the scaled-up model can be used. It can be stated that with introducing higher chamfer at the nozzle hole inlet the quantity of vapour is lowered. In sharp edge case (Case 6) the vapour is spreading almost through one half of the hole and it is also present at the lower inlet edge. In cases 7 and 8 there is less vapour present and the predicted volume fractions are more or less in the region under the 0.5. In Case 9 (r=0.15 mm) there is almost no vapour present, while at the Case 10 (r=0.20 mm) vapour completely vanishes from the nozzle. When comparing the discharge coefficients it can be stated that introducing higher chamfer radii significantly changes the values of the coefficient. In case 6 the value of discharge coefficient equals 0.466, in cases 7 and 8 it is 0,577 and 0.630 respectively. The difference between cases 9 and 10 is not significant. The values are 0.657 and 0.662 respectively.

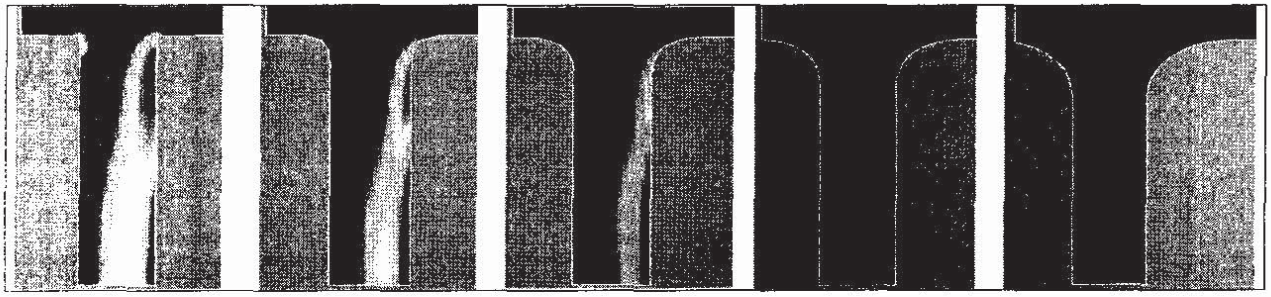

Figure 4.6. Vapour volume fraction in the nozzle, side view, centre cut (from left: case 6-10)

Similar results as in previous case were obtained also at the single-phase numerical analysis made on three-dimensional one-quarter model of the real nozzle. The results showed that the introduction of round inlet edges can significantly lower the separation of the flow. The analyses were made for the nozzle hole with diameter 0.375 mm. The inclination angle of the hole was 95°.

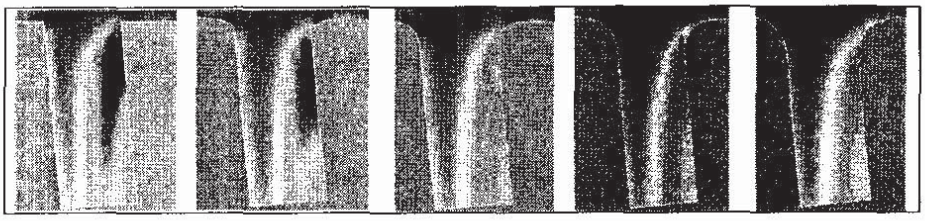

Figure 4.7. Pressure distribution in the nozzle hole at different inlet radius (central cut, from left: sharp edge, 0.05, 0.1, 0.15 and 0.2 mm, Scaling: dark colours-low pressure regions, light colours –high pressure)

The pressure distributions presented on Figure 4.7 show that the very low pressure area in the re-circulation zone vanishes by introducing higher inlet radius. The discharge coefficient rises from the value of 0.746 at sharp edge up to 0.839 at the 0.2 mm chamfer radius. This also means, that the velocity at the outlet is higher and it is also more uniform. Higher output velocities result also in better atomisation of injected fuel. This phenomenon should be observed more carefully, since several authors (for example [4], [8], [14], [20]) also discussed the positive influence of the cavitation on the spray formation. Thus we could only clearly demonstrate that the introduction of the chamfer at the nozzle inlet lowers the possibility of the material damages due to cavitation. On the other side it should be also mentioned that the production of the inlet chamfers is limited to some extent.

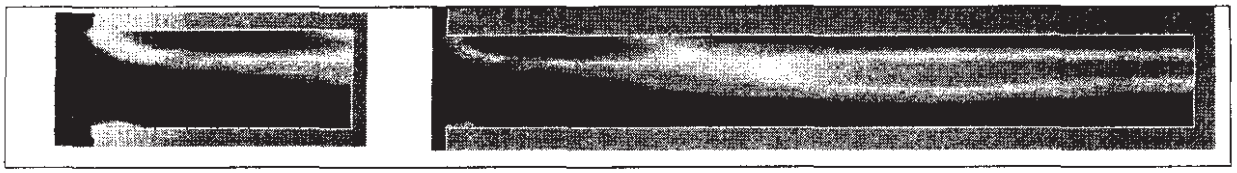

Figure 4.8. Vapour volume fraction in nozzle hole, centre cut, left -Case 11, right – Case 12

The vapour volume fraction for cases 11 and 12 are presented on Figure 4.7. When comparing the results of Case 6, 11 and 12 the following can be observed. The structure of the cavitation is not dependent on the length of the nozzle hole. The shape of cavitation in the first part of the hole is almost identical in all three cases; later on the vapour cloud is spreading through the hole till it reaches the outlet. There is almost no change of the discharge coefficient between all three cases. From those first analyses no concrete conclusion can be made. We can only speculate that shorter nozzle hole might have a good influence on the spray formation, since at other cases the back flow of the gas could be observed to some extent. Further we can also suppose that in region where the vapour volume fraction is lowered significantly (about 0.6 mm from the nozzle hole inlet) some damages due to the bubble collapse can be expected.

5. Conclusions

Considering above-mentioned results the following conclusions can be made:

- The numerical analysis on scaled-up model shows that higher pressure differences yield more cavitation. Cavitation could even reach the outlet of the hole.
- The results of the numerical analysis are comparable to the experimental results on the same scaled-up model (See Ganippa [8]).
- By introducing the chamfer at the inlet edges of the nozzle hole the cavitation can be lowered significantly.
- First analyses show no significant influence of the nozzle hole length on the shape of the cavitation.

References

[1] C.Arcoumanis et. al., Visualisation of cavitation in diesel engine injectors, Mec.Ind. (2001) 2, 375-381

[2] C.Arcoumanis et.al., Investigation of cavitation in a vertical multi-hole injector, SAE paper 1999-01-0524

[3] C.Arcoumanis et.al, Cavitation in real-size multi-hole diesel injector nozzles, SAE paper 2000-01-1249

[4] C.Badock et.al, Investigation of cavitation in real size diesel injection nozzle, International Journal of Heat and Fluid Flow 20 (1999)

[5] C.Baumgarten et.al., Numerical and experimental investigations of cavitating flow in high pressure diesel nozzles, ILASS-Europe 2001, Zurich

[6] E.v.Berg et.al., Validation of a CFD model for coupled simulation of nozzle flow, primary fuel jet break-up and spray formation, ICES2003-643, 2003 Spring Technical Conference of the ASME Internal Combustion engine Division, Salzburg, 2003

[7] FIRE Version 8 – Users manual, Multiphase flow, AVL, 2003

[8] L.C.Ganippa et.al., The structure of cavitation and its effect on the spray pattern in a single hole diesel nozzle, SAE paper 2001-01-2008

[9] L.C.Ganippa et.al.,Comparison of cavitation phenomena in transparent scaled-up single hole diesel nozzles, 4th international symposium on cavitation, California institute of technology, Pasadena, 2001
[10] B.Göschel, Einspritzdüsenverschleiß, Forschungverinigung Verbrenungskraftmachinen e.V., Heft R245, 1974
[11] K.Jung et.al., The breakup characteristics of liquid sheets formed by like-doublet injectors, Journal of Propulsion and Power (sent), http://rpl.snu.ac.kr/
[12] Kavitation. Abschlüßberichtüber die Ergebnise des Schwerpunktprogramm 1966-1972, Deutsche Forschungsgemeinschafts, Boppard, 1974
[13] G.König et.al., Analysis of flow and cavitation Phenomena in diesel injection nozzles and its effects on spray and mixture formation, 5.Internationales Symposium für Verbrennungsdiagnostik der AVL Deutschland, 6.-7.Juni 2002, Baden Baden, 2002
[14] Y.Laoonual et.al., Internal fluid flow and spray visualization for a large scale valve covered orifice (VCO) injector nozzle, ILASS-Europe 2001, Zurich, 2-6 September, 2001
[15] K.Melcher, I.Komaroff, Experimentelle Utersuchung der Stroemung durch Dieseleinspritzduesen in stationaer betriebenen Grossmodel, Bosch Techn. Berichte 5 (1976) 4
[16] W.H.Nurrick, Orifice cavitation and its effects on spray mixing, Journal of fluids Engineering, 98 (1976)
[17] R.Payri. et.al., The influence of cavitation on the internal flow and the spray characteristics in diesel injection nozzles, FUEL 83 (2004)
[18] J.Sauer, Instationaer kavitirende Stroemungen – Ein neues Modell, basierend auf Front Capturing (VoF) und Blasendynamik, PhD Thesis, Unversitaet Karlsruhe, Karlsruhe, 2000
[19] D.P.Schmidt et.al., Analyitical prediction of the exit flow of the cavitating flow, Atom. and sprays, 6 (1997)
[20] C.Soteriou et.al., Through the diesel nozzle hole–a journey of discovery II, ILASS-Europe 2001, Zurich
[21] E.Winklhofer et.al, Basic flow processes in high pressure fuel injection equipment, Proceedings of the 9th International conference on liquid atomization and spray systems, ICLASS-2003, Sorento, Italy, July (2003)